930 J. Med. Chem. 2011, 54, 930–938
DOI: 10.1021/jm1010836

Journal of Medicinal Chemistry Article

X-ray Crystal Structure and Binding Mode Analysis of Human *S*-Adenosylhomocysteine Hydrolase Complexed with Novel Mechanism-Based Inhibitors, Haloneplanocin A Analogues†

Kang Man Lee,‡ Won Jun Choi,§,∥ Yoonji Lee,‡ Hyun Joo Lee,‡ Long Xuan Zhao,‡,⊥ Hyuk Woo Lee,§ Jae Gyu Park,‡ Hea Ok Kim,‡ Kwang Yeon Hwang,# Yong-Seok Heo,∞ Sun Choi,*,‡ and Lak Shin Jeong*,‡,§

‡*College of Pharmacy, and* §*Department of Bioinspired Science, Ewha Womans University, Seoul 120-750, Korea,* ∥*College of Pharmacy, Dongguk University, Kyungki-do 410-774, Korea,* ⊥*College of Chemistry and Chemical Engineering, Liaoning Normal University, Dalian 116-029, China,* #*College of Life Sciences and Biotechnology, Korea University, Seoul 136-701, Korea, and* ∞*Department of Chemistry, Konkuk University, Seoul 143-701, Korea*

Received August 21, 2010

The X-ray crystal structure of human *S*-adenosylhomocysteine (AdoHcy) hydrolase was first determined as a tetrameric form bound with the novel mechanism-based inhibitor fluoroneplanocin A (**4b**). The crystallized enzyme complex showed the closed conformation and turned out to be the intermediate of mechanism-based inhibition. It confirmed that the cofactor depletion by 3′-oxidation of fluoroneplanocin A contributes to the enzyme inhibition along with the irreversible covalent modification of AdoHcy hydrolase. In addition, a series of haloneplanocin A analogues (**4b**−**e** and **5b**−**e**) were designed and synthesized to characterize the binding role and reactivity of the halogen substituents and the 4′-CH_2OH group. The biological evaluation and molecular modeling studies identified the key pharmacophores and structural requirements for the inhibitor binding of AdoHcy hydrolase. The inhibitory activity was decreased as the size of the halogen atom increased and/or if the 4′-CH_2OH group was absent. These results could be utilized to design new therapeutic agents operating via AdoHcy hydrolase inhibition.

Introduction

S-Adenosylhomocysteine (AdoHcy[a]) hydrolase[1] is an important cellular enzyme catalyzing the hydrolysis of *S*-adenosylhomocysteine to adenosine and L-homocysteine and an attractive target for the development of broad-spectrum antiviral agents.[2] The antiviral activity resulting from the inhibition of AdoHcy hydrolase is associated with the feedback inhibition of *S*-adenosyl-L-methionine-dependent transmethylase, which is essential for the formation of the capped methylated structure at the 5′-terminus of viral mRNA.

There have been AdoHcy hydrolase inhibitors synthesized and evaluated for their activities, and two types of mechanism-based inhibitors of AdoHcy hydrolase are reported.[3] Type I mechanism-based inhibitors inactivate the enzyme by converting the cofactor NAD^+ to NADH, resulting in the depletion of NAD^+.[3] This type of inhibition is reversible on incubation with an excess amount of NAD^+ or on dialysis. Type II mechanism-based inhibitors not only deplete the cofactor NAD^+ as type I inhibitors do but also bind covalently with the nucleophilic amino acid residue at the active site, resulting in the permanent irreversible inhibition of the enzyme.[3] Thus, the catalytic activity of the enzyme is not restored even after dialysis or incubation with NAD^+.

Neplanocin A (X = CH_2OH, Y = H) is a highly potent and reversible inhibitor of AdoHcy hydrolase.[4] It is oxidized to its 3′-keto form by NAD^+ bound to AdoHcy hydrolase, and it maintains the cofactor permanently in the reduced form (i.e., NADH),[3,4] causing type I mechanism-based inhibition. We recently designed and synthesized fluoroneplanocin A (X = CH_2OH, Y = F), containing a leaving group fluorine atom in place of hydrogen at C6′, and it turned out to be a more potent inhibitor of AdoHcy hydrolase than neplanocin A.[5] The dialysis, incubation with NAD^+, and ^{19}F NMR experiments indicated that fluoroneplanocin A works as an irreversible mechanism-based inhibitor. Interestingly, it showed the biphasic kinetic behavior, and ^{19}F NMR experiments revealed that the ratio of the released fluoride anion to the used enzyme was not stoichiometric, indicating that the conversion of the intermediate **1** to the final adduct **3** (Scheme 1) might not be completely irreversible when the deprotonation of the intermediate **2** results in the elimination of the enzyme instead of the fluoride anion. Thus, it was hypothesized that the additional type I reversible inhibition by intermediate **1**, along with type II irreversible inhibition, may be involved in the mechanism-based inhibition of AdoHcy hydrolase.

In order to confirm the additional type I reversible inhibition, we obtained the X-ray crystal structure of human AdoHcy hydrolase complexed with the fluoroneplanocin A. On the basis of this X-ray crystal structure of human AdoHcy hydrolase, a series of haloneplanocin A analogues **4** were

†The atomic coordinates and structure factors for the crystal structure of human AdoHcy hydrolase complexed with compound **4b** have been deposited in the Protein Data Bank with accession code 3NJ4.

*To whom correspondence should be addressed. For S.C.: phone, 82-2-3277-4503; fax, 82-2-3277-2851; e-mail, sunchoi@ewha.ac.kr. For L.S.J.: phone, 82-2-3277-3466; fax, 82-2-3277-2851; e-mail, lakjeong@ewha.ac.kr.

[a] Abbreviations: AdoHcy, *S*-adenosyl-L-homocysteine; NAD, nicotinamide adenine dinucleotide; NFSI, *N*-fluorobenzenesulfonimide; GOLD, genetic algorithm of ligand docking; rmsd, root means square deviation.

 Published on Web 01/12/2011

Scheme 1. Proposed Mechanism-Based Inhibition of AdoHcy Hydrolase by Haloneplanocin A Analogues

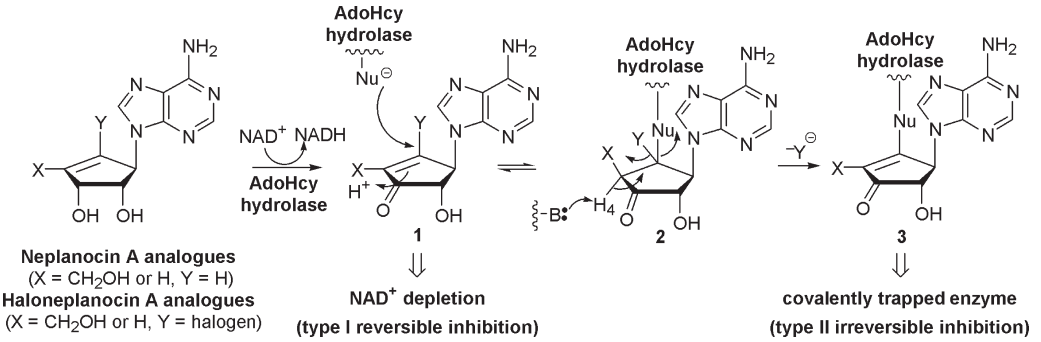

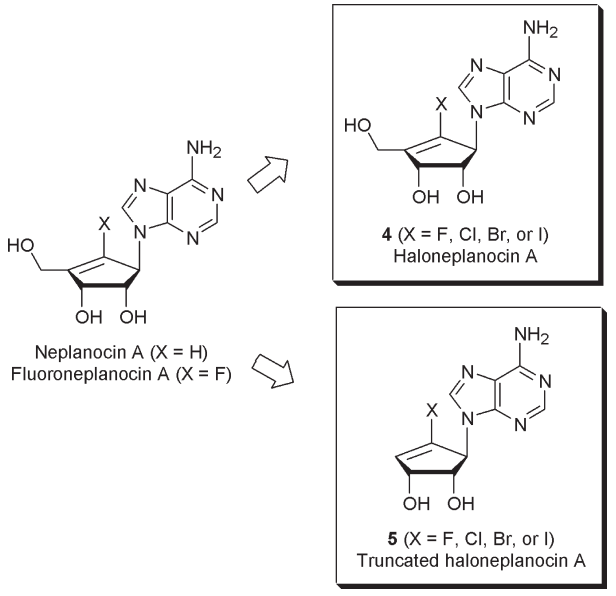

Figure 1. Haloneplanocin A (**4**) and truncated haloneplanocin A (**5**) designed for the identification of the pharmacophores of AdoHcy hydrolase.

designed and synthesized to determine the effect of halogen in binding at the active site of AdoHcy hydrolase (Figure 1). A series of truncated haloneplanocin A analogues **5** were also designed and synthesized to identify if the 4′-CH_2OH group serves as the key pharmacophore in the active site of AdoHcy hydrolase. We also performed the molecular docking study of the synthesized nucleosides to the X-ray crystal structure of AdoHcy hydrolase to study the correlation between the AdoHcy hydrolase inhibitory activity (IC_{50}) and binding energy. Herein, we report the full accounts of design, synthesis, and molecular modeling studies of haloneplanocin A (**4**) and truncated haloneplanocin A (**5**) to reveal the key pharmacophores and structural requirements for the inhibitor binding of AdoHcy hydrolase.

Results and Discussion

Chemistry. A series of halogenated neplanocin A analogues **4** (X = CH_2OH, Y = F, Cl, Br, or I)[6] were designed and synthesized to characterize the binding role and reactivity of the halogen substituents. The corresponding 4′-CH_2OH truncated analogues **5** (X = H, Y = H, F, Cl, Br, or I)[6] were also prepared to find out the binding role of the 4′-CH_2OH group at the active site of AdoHcy hydrolase.

Our synthetic strategy to haloneplanocin A analogues **4** and truncated haloneplanocin A analogues **5** was to synthesize the glycosyl donors **14** and **15** and then to condense them with adenine, as shown in Scheme 2. D-Ribose was efficiently converted to the key intermediates, cyclopentenone derivatives **6** (X = CH_2OBn) and **7** (X = H), according to our published procedures.[7,8] Halogenation of cylcopentenone derivatives **6** (X = CH_2OBn)[8] and **7** (X = H)[7] using Cl_2, Br_2, or I_2 in pyridine afforded the halogenated cyclopentenone derivatives **8** (X = CH_2OBn, Y = Cl, Br, or I) and **9** (X = H, Y = Cl, Br, or I), respectively. For the introduction of fluorine atom on the α position of α,β-unsaturated ketone, iodocyclopentenones **8** (X = CH_2OBn, Y = I) and **9** (X = H, Y = I) were stereoselectively reduced with $NaBH_4$ to give the iodocyclopentenols, which were treated with TBDPSCl to give the TBDPS protected derivatives **10** (X = CH_2OBn, Y = I) and **11** (X = H, Y = I), respectively. Treatment of **10** (X = CH_2OBn, Y = I) and **11** (X = H, Y = I) with *N*-fluorobenzenesulfonimide (NFSI) in the presence of *n*-BuLi at −78 °C yielded α-fluorinated derivatives **12** (X = CH_2OBn, Y = F)[5] and **13**[9] (X = H, Y = F), respectively, after the removal of TBDPS group. For the synthesis of other halogen derivatives (Y = Cl, Br, or I), compounds **8** (X = CH_2OBn, Y = Cl, Br, or I) and **9** (X = H, Y = Cl, Br, or I) were reduced with $NaBH_4$ to give other halogenated alcohols **12** (X = CH_2OBn, Y = Cl, Br, or I) and **13** (X = H, Y = Cl, Br, or I), respectively. The allylic alcohol derivatives **12** (X = CH_2OBn, Y = F, Cl, Br, or I) and **13** (X = H, Y = F, Cl, Br, or I) were converted to the glycosyl donors **14** (X = CH_2OBn, Y = F, Cl, Br, or I) and **15** (X = H, Y = F, Cl, Br, or I), which were condensed with adenine anion in DMF to give the condensed products **16** (X = CH_2OBn, Y = F, Cl, Br, or I) and **17** (X = H, Y = F, Cl, Br, or I). Removal of benzyl and acetonide protecting groups of **16** (X = CH_2OBn, Y = F, Cl, Br, or I) with boron trichloride afforded the final haloneplanocin A analogues **4** (X = CH_2OH, Y = F, Cl, Br, or I). Treatment of **17** (X = H, Y = F, Cl, Br, or I) with 70% TFA afforded the truncated haloneplanocin A analogues **5** (X = H, Y = F, Cl, Br, or I).

Enzyme Assay. All the final nucleosides **4** and **5** were assayed for the AdoHcy hydrolase inhibitory activities using pure recombinant human placental AdoHcy hydrolase obtained from *E. coli* JM109 containing the plasmid pPROKcd20.[5] Compounds **4** and **5** were preincubated with the AdoHcy hydrolase at various concentrations for 5−10 min at 37 °C, and the residual activity of the enzyme was measured in the synthetic direction toward *S*-adenosylhomocysteine using adenosine and L-homocysteine.

Most of the synthesized compounds showed potent inhibitory activity against the AdoHcy hydrolase, as shown in Table 1, and all these active compounds (**4b**−**d** and **5b**) inhibited the AdoHcy hydrolase in concentration- and time-dependent manners (Figure S1 and S2 in the Supporting

Scheme 2. Synthesis of the Final Nucleosides **4** and **5** from D-Ribose

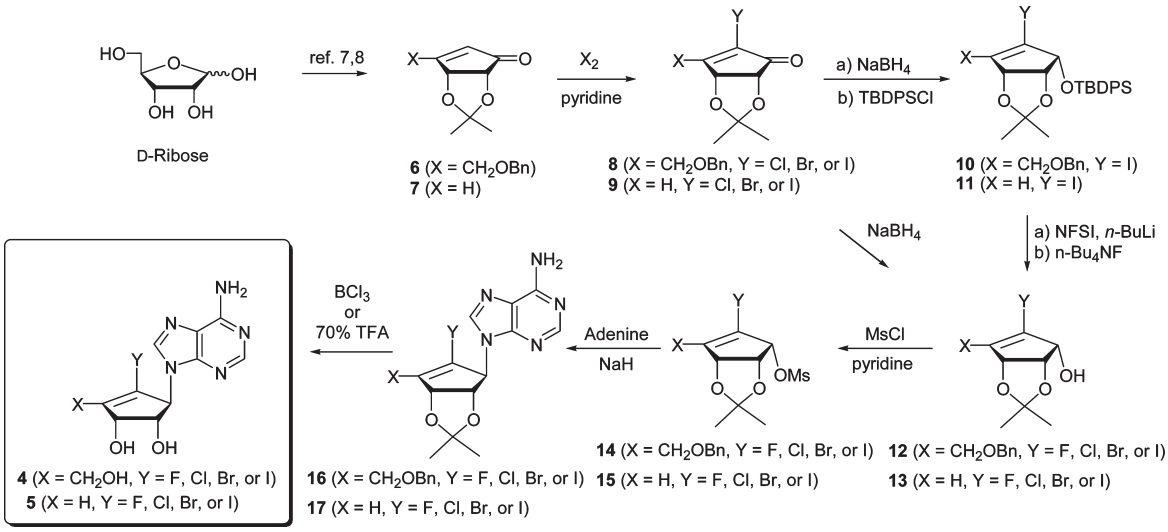

Table 1. AdoHcy Hydrolase Inhibitory Activity of Neplanocin A (**4a**), Haloneplanocin A Analogues **4b**−**e**, Truncated Neplanocin A (**5a**), and Truncated Haloneplanocin A Analogues **5b**−**e**

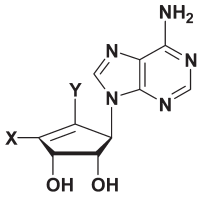

4a-**e** (X = CH_2OH, Y = H, F, Cl, Br, or I)
5a-**e** (X = H, Y = H, F, Cl, Br, or I)

compd (X, Y)	IC_{50} (μM)	compd (X, Y)	IC_{50} (μM)
4a (X = CH_2OH, Y = H)	0.87	**5a** (X = H, Y = H)	5.83
4b (X = CH_2OH, Y = F)	0.48	**5b** (X = H, Y = F)	7.67
4c (X = CH_2OH, Y = Cl)	36.46	**5c** (X = H, Y = Cl)	> 1000
4d (X = CH_2OH, Y = Br)	60.17	**5d** (X = H, Y = Br)	> 1000
4e (X = CH_2OH, Y = I)	> 1000	**5e** (X = H, Y = I)	> 1000

Information). Fluoroneplanocin A (**4b**) exhibited the most potent enzyme inhibitory activity (IC_{50} = 480 nM), which is ~2-fold more potent than neplanocin A (**4a**). Other haloneplanocin A analogues were designed with better leaving groups (i.e., Cl, Br, and I) and expected to have higher activities because the carbon−halogen bonds of other haloneplanocin A analogues could be cleaved more easily than the carbon−fluorine bond during the mechanism-based inhibition of AdoHcy hydrolase if they bind at the active site. Surprisingly, the activities of the halo analogues tend to be gradually diminished as the size of halogen atom increased in the order of Cl, Br, and I. Especially, the iodo derivative (**4e**) showed that it is less likely to bind to AdoHcy hydrolase despite having the best leaving group. Since the biological activity of this series of mechanism-based inhibitors could be the net effect of how well the ligand binds and how reactive the bound ligand is, these results indicated that the proper ligand binding seems to be more critical than the chemical reactivity for the activity in this series of inhibitors.

In order to determine whether the 4′-CH_2OH group is important for binding, the truncated haloneplanocin A **5b**−**e** were synthesized and tested. They showed much lower potency compared with the corresponding 4′-CH_2OH-containing compounds. The truncated neplanocin A (**5a**) and its fluorinated compound (**5b**) have low micromolar range of IC_{50} values, but chloro, bromo, and iodo derivatives (**5c**, **5d**, and **5e**) are unlikely to bind at all. Since the 4′-CH_2OH group seems to be one of the key pharmacophores for the binding with AdoHcy hydrolase, the substituent increasing a hydrogen bonding capacity may improve the inhibitory activity against AdoHcy hydrolase. This assumption was confirmed by the X-ray crystal structure of AdoHcy hydrolase complexed with fluoroneplanocin A (**5b**) in the following part.

The irreversibility of inactivation for compounds **4c**−**e** and **5c**−**e** was confirmed by dialysis as in the case of **4b**[5] and **5b**.[9] The level of inhibition of AdoHcy hydrolase obtained after preincubation of the enzyme at various inhibitory concentrations of each compound remained unchanged after dialysis (Figure S3 in the Supporting Information).

X-ray Crystal Structure of AdoHcy Hydrolase Complexed with Fluoroneplanocin A. In order to understand the binding mode of the inhibitor at the molecular level, human AdoHcy hydrolase was crystallized with the most potent inhibitor, fluoroneplanocin A, along with the cofactor NAD^+. This is the first reported X-ray crystal structure of human AdoHcy hydrolase as a tetrameric form (Figure 2a).

Four subunits are connected around the pseudo-222 symmetry to form a tetramer, where each monomer is occupied by the cofactor and the ligand. The monomeric subunit of AdoHcy hydrolase is composed of the catalytic domain, the cofactor-binding domain, and the C-terminal domain (Figure 2b). The catalytic and cofactor-binding domains are linked by the α-helix, which might serve as a molecular hinge. The final refined X-ray crystal structure showed that it formed a strong ternary complex of the inhibitor, AdoHcy hydrolase, and NADH. Interestingly, the crystallized enzyme−ligand complex turned out to be the intermediate of the inhibition, bound with fluoroneplanocin A oxidized in its 3′-position (i.e., **1** in Scheme 1) by the cofactor NAD^+, and its electron density map is as shown in Figure 2c. Taken together with our previous report that fluoroneplanocin A inhibits AdoHcy hydrolase irreversibly and its fluorine atom is extracted after the incubation with the enzyme,[5] it might function by dual inhibition: the cofactor depletion and covalent modification of the enzyme.

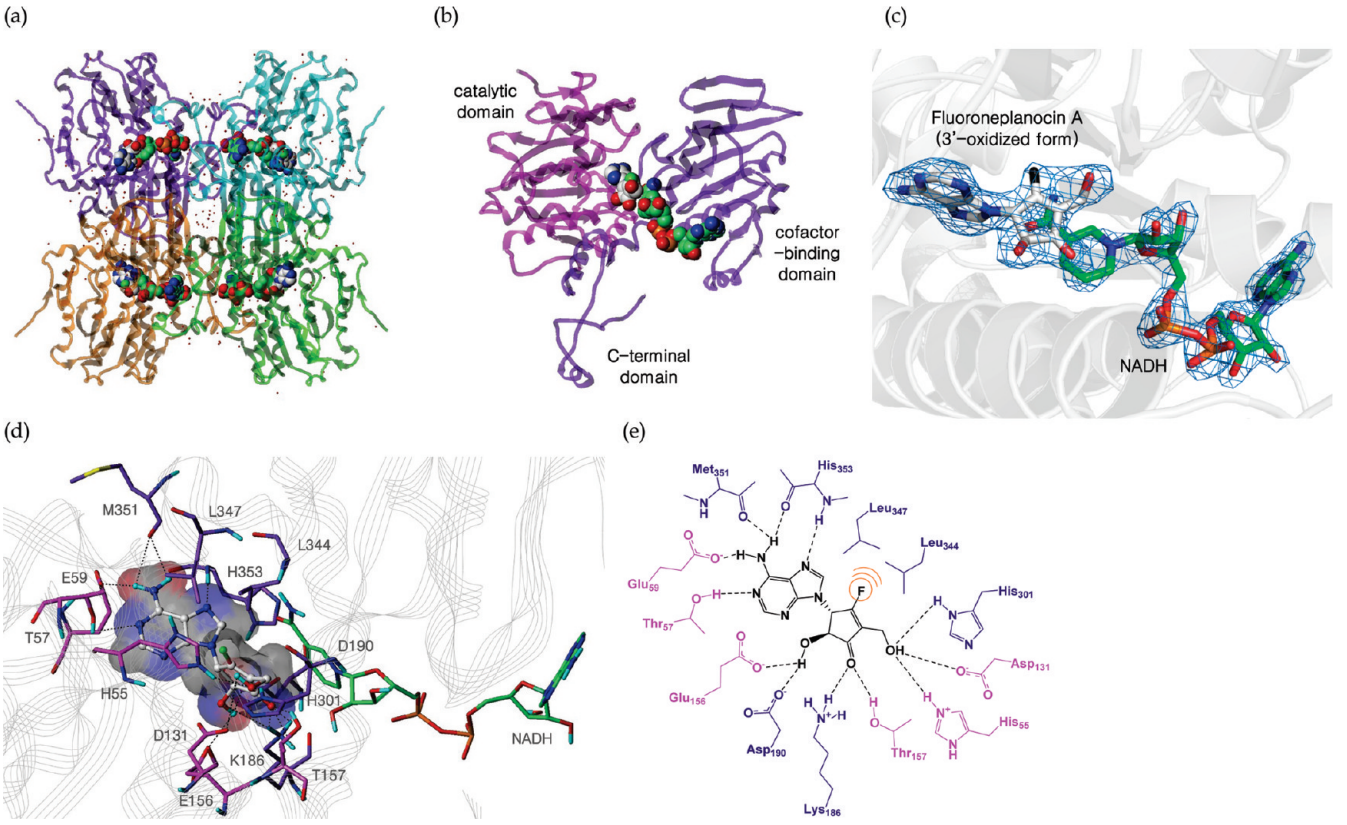

Figure 2. X-ray crystal structure of AdoHcy hydrolase complexed with fluoroneplanocin A. (a) Homotetrameric topology of human AdoHcy hydrolase. Each monomer is shown in the secondary structure colored by purple, cyan, orange, and green, with the water molecules displayed as balls. The ligand and the cofactor molecules are represented in spacefill, and their carbon atoms are in white and green, respectively. (b) Monomeric subunit consisting of the catalytic domain, the cofactor-binding domain, and the C-terminal domain. (c) σ_A-weighted $2F_o - F_c$ electron density map calculated with a final refined model of the structure without fluoroneplanocin A and NAD^+ at a level of 1.2σ. The carbon atoms of fluoronecplanocin A and NADH are in white and green, respectively, and the fluorine atom is in black. (d) Fluoroneplanocin A with the key binding residues at the enzyme active site. The ligand is depicted as ball-and-stick with carbon atoms in white. Its van der Waals surface was generated by MOLCAD and colored by hydrogen bonding property (red, H-bond donating regions; blue, H-bond accepting regions). (e) Schematic diagram of the binding interactions of fluoroneplanocin A at the active site of AdoHcy hydrolase. Interacting residues in the cofactor-binding domain and the catalytic domain are represented in purple and magenta, respectively. The hydrophobic interactions are colored in orange, and the hydrogen bondings are displayed as dashed lines.

The binding interactions of fluoroneplanocin A at the active site of AdoHcy hydrolase is as shown in Figure 2d. Its overall binding mode is retained as that of neplanocin A,[10] including the hydrogen bondings with His55, Thr57, Glu59, Asp131, Glu156, Thr157, Lys186, Asp190, His301, Met351, and His353. In addition, there is a hydrophobic interaction between the fluorine atom and the active site hydrophobic pocket, contributed by the two Leu residues (i.e., Leu344 and Leu347). It might be one of the reasons why fluoroneplanocin A is more potent than neplanocin A. In the dimer structure, the cofactor-binding domain of a monomer has an interface interacting with the α-helix of its dimer partner. Binding of the cofactor NAD^+ to AdoHcy hydrolase requires the contributions from both dimer subunits, unlike NAD-dependent dehydrogenases where each cofactor is typically bound in one monomer exclusively.[11] Also, the C-terminal domains are exchanged between the adjacent dimer partners and accommodate part of the cofactor-binding sites.[12] Overall, a dimer of the enzyme is required to form a complete cofactor-binding site.[11]

The dimer itself, however, is not sufficient to establish a strong rigid core framework. Therefore, AdoHcy hydrolase is assembled into a tetrameric form.[12] The four cofactor-binding domains are tightly linked together at the center of the tetramer and make it possible to build up the core structure. Besides, the catalytic domains are connected with the cofactor-binding domains via hinge regions. They are located on the periphery of the tetramer and have little interaction with one another. So, architecturally, the tetrameric structure indicates that the catalytic domains are more mobile compared with the cofactor-binding domains. In fact, it was reported that the average temperature factor of the catalytic domain is significantly higher than that of the cofactor-binding domain,[12] and our human AdoHcy hydrolase X-ray crystal structure also confirmed this finding. Overall, the tetramer formation appears to allow the enzyme to build a strong and rigid molecular framework as well as flexible catalytic sites.

Regarding the conformation of AdoHcy hydrolase, there are two distinct forms: open and closed. In the resting state, the catalytic and cofactor-binding domains are opened through 19° to expose the active site to the environment.[10] Upon ligand binding, AdoHcy hydrolase makes a substantial conformational change. The ligand seems to bind to the catalytic domain first and then move along with the relatively mobile catalytic domain to acquire the interactions with the cofactor-binding domain as depicted in Figure 2e.

As a result, the enzyme forms the closed conformation. Compared with our open form homology model (Figure 3a),

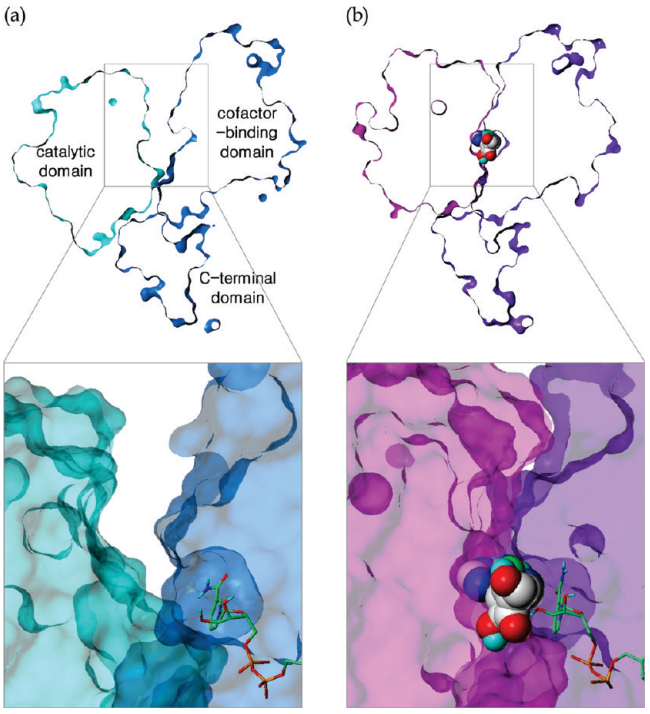

Figure 3. Comparison of the open and closed forms of human AdoHcy hydrolase. (a) Homology model of the open form human AdoHcy hydrolase. (b) X-ray crystal structure of the closed form human AdoHcy hydrolase with fluoroneplanocin A bound between the catalytic and cofactor-binding domains. Connolly surface was generated and Z-clipped from both the front and back sides (in the upper view) and from the front side only (in the bottom view). In the open form structure, the catalytic domain is colored by cyan and the cofactor-binding and C-terminal domains are in sky blue. In the closed form structure, they are in magenta and purple, respectively. Fluoroneplanocin A is displayed in spacefill and the cofactor is in capped-stick with their carbon colors of white and green-blue, respectively. The nonpolar hydrogen atoms are not displayed for clarity.

the crystal structure of human AdoHcy hydrolase complexed with fluoroneplanocin A has the closed conformation, making the ligand completely embraced between the two domains, and forms the strong ternary complex of the inhibitor, AdoHcy hydrolase, and NADH (Figure 3b).

In addition, our X-ray crystal structure of human AdoHcy hydrolase was compared with those of other species. Their sequence identities and rmsd values were measured, and the overall structures appeared to be very similar (Table S1 and Figure S4 in the Supporting Information). The only difference is the additionally inserted helix−loop−helix structure, which was reported to be present within the catalytic domain in most of bacteria and some eukaryotes but not in mammals.[13] The active site residues of AdoHcy hydrolases are highly conserved, and their 3D structures are very similar (Figure S5 in the Supporting Information). It would be challenging to achieve the ligand selectivity among different species, but it was reported that introducing the functional group at the C2 position of adenine ring could achieve the selectivity due to the difference of Thr60 in human and Cys59 in *Plasmodium falciparum* AdoHcy hydrolases[14] (Figure S6 in the Supporting Information).

Molecular Modeling Analysis. To investigate the binding modes of the series of haloneplanocin A analogues, flexible docking studies were performed. While the X-ray crystal structure was prepared, all hydrogen atoms were added and the protonation state of the ionizable groups was chosen appropriate to pH 7.0. According to Yamada et al.,[15] His54 residue in rat appears to be protonated in its N_{E2} position and the protonation state of this residue is less influenced by the pH of solution. So His55 residue was prepared to be protonated for the molecular modeling studies. Then the flexible docking was performed using the GOLD (genetic algorithm of ligand docking) program, version 4.1. To consider the protein flexibility, 10 residues interacting with the ligand at the active site were selected and set to be flexible. Each inhibitor structure was prepared as the oxidized form in its 3′-position and docked into the protein structure in the presence of NADH. The GOLD fitness scores of the docked molecules had good correlation with their biological activities. Among the docking results, the reasonable complexes with high GOLD fitness scores were selected and energy minimized with the conjugate gradient algorithm using CHARMm program. After the energy minimization, conformations of the docked ligands did not change so much but the whole systems were relaxed to the more stable structures. The docked and energy-minimized conformations of the analogues were shown in Figure 4.

The adenine part of the analogues was docked almost exactly the same way, maintaining the bidentate hydrogen bonding with Thr57 and Glu59. However, the position of the cyclopentenyl ring was prone to be pushed away from the hydrophobic pocket, which could accommodate the halogen atom, as the size of the halogen atom increased. The van der Waals radius of hydrogen is 1.20 Å, and those of halogen atoms are 1.47 Å for fluorine, 1.75 Å for chlorine, 1.85 Å for bromine, and 1.98 Å for iodine.[16] The surface representation of each complex clearly showed the conformational adjustment of the compounds to fit into the active site cavity (Figure 4a). In the case of iodoneplanocin A, the bulkiness of the iodine atom seemed to cause too much of shifting for the cyclopentenyl ring and lose the hydrogen bonding with His301 (Figure 4b). These results demonstrate that there is a spatial limitation of the small and rigid hydrophobic pocket where the halogen atoms could be positioned. Thus, unlike fluoroneplanocin A (**4b**), iodoneplanocin A (**4e**) appears not to maintain the appropriate conformation for binding at the active site and shows no activity in spite of having the most reactive leaving group in this series. Therefore, the ligand binding might be the more important factor than the chemical reactivity for the inhibitory activity of this series of haloneplanocin A analogues. Also, the 4′-CH_2OH group played a crucial role in the binding of neplanocin A and haloneplanocin A analogues through the key hydrogen bondings with the active site His301. Consequently, the 4′-CH_2OH truncated analogues lost the activity to 1 order of magnitude or more compared with their counterparts (Table 1).

In addition, the binding energy was calculated for each ligand−enzyme complex. For the calculation of the relative binding energy of a ligand, it is necessary to consider the structural changes between the holoenzyme in the open conformation and the ligand-bound enzyme in its closed conformation. The binding energies of neplanocin A and haloneplanocin A analogues were calculated using the docked and energy-minimized systems for the ligand-bound structures and the refined homology model for the holoenzyme structure. The total energy of each system was calculated using CHARMm energy function and the implicit solvent model, generalized Born with molecular volume (GBMV).

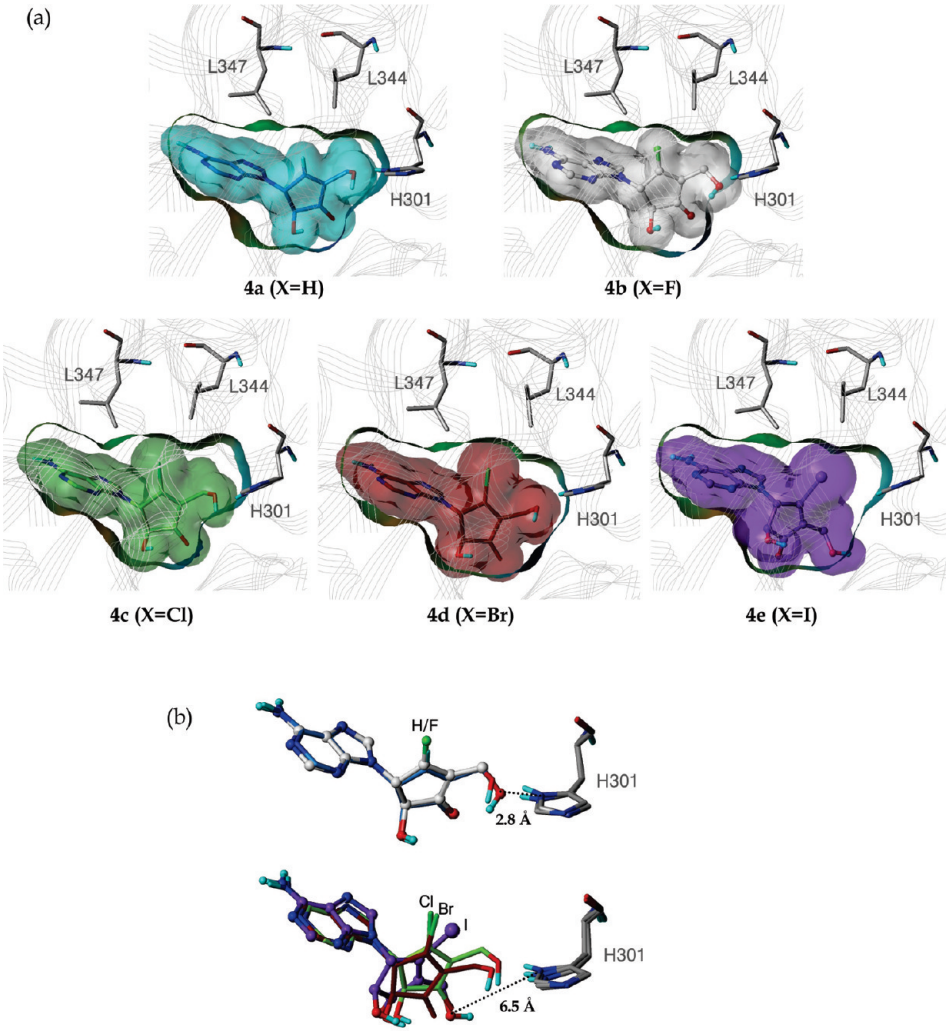

Figure 4. Binding modes of neplanocin A (**4a**) and haloneplanocin A analogues **4b**−**e**. (a) Flexible docked and energy-minimized conformations of the analogues at the enzyme active site. (b) Comparison of the ligand conformations aligned by the ligand-bound enzyme complexes (with His301 displayed). Neplanocin A (**4a**) and fluoroneplanocin A (**4b**) are displayed in capped-stick with its carbon color of sky blue and in ball-and-stick with its carbon color of white, respectively. Chloro- and bromoneplanocin A (**4c** and **4d**) are depicted in capped-stick, and their carbons are in green and brown, respectively. Iodoneplanocin A (**4e**) is shown in ball-and-stick with its carbon color of purple. His301, Leu344, and Leu347 residues in each complex are displayed in capped-stick with the carbons in gray. The distances between His301 (N_{D1}) and the 5′-oxygens of fluoroneplanocin A and iodo-neplanocin A are 2.8 and 6.5 Å, respectively. The nonpolar hydrogen atoms, except the 6′-hydrogen of neplanocin A (**4a**), are not displayed for clarity. The fast Connolly surface of the protein and the van der Waals surface of the ligands were generated by MOLCAD. The protein surface is colored by lipophilicity and Z-clipped, and each ligand surface is in its carbon color.

Table 2. Calculated Average Binding Energies of Neplanocin A (**4a**) and Haloneplanocin A Analogues **4b**−**e**

compd	X	IC_{50} (μM)	binding energy (kcal/mol)
4a	H	0.87	−53.24
4b	F	0.48	−65.03
4c	Cl	36.46	−43.23
4d	Br	60.17	−30.83
4e	I	>1000	−8.75

For more efficient calculation, binding energies were estimated using the following formula:

$$\text{binding energy} = E_{\text{complex}} - E_{\text{holoenzyme}} - E_{\text{free ligand}} \quad (1)$$

The binding energies of the tested compounds showed good correlation with their IC_{50} values; as the binding energies increased, the IC_{50} values also increased (Table 2).

For neplanocin A and fluoroneplanocin A, the binding energies are very low and it means that the complexes are very stable when these ligands are bound to the enzyme. On the other hand, the binding energy of iodo derivative is very high, indicating that the enzyme complex with this ligand would be energetically unstable.

Conclusion

The X-ray crystal structure of human AdoHcy hydrolase, complexed with the novel mechanism-based inhibitor fluoroneplanocin A, was first determined, and it confirmed the additional type I reversible mechanism. Considering the irreversible nature of inhibition by fluoroneplanocin A, it was elucidated that the enzyme inhibition of fluoroneplanocin A is involved in the dual mechanism: the cofactor depletion and covalent modification of the enzyme. In addition, the crystallized protein−ligand complex shows that the inhibitor induces the open-to-closed conformational change. It makes the ligand possible to bind tightly between the cofactor-binding and

catalytic domains and form the strong ternary complex of the inhibitor, AdoHcy hydrolase, and NADH, allowing the mechanism-based inhibition reaction to occur. Moreover, we identified the key pharmacophores and structural requirements for inhibitor binding through the biological evaluation and molecular modeling studies of the synthesized haloneplanocin A and the corresponding truncated analogues. This kind of comprehensive study, based on chemistry, structural biology, and molecular modeling, gave insight for the inhibitor design, and these results will be utilized for the discovery of new therapeutic agents.

Experimental Section

General Methods. ^{1}H NMR spectra ($CDCl_3$, CD_3OD, or DMSO-d_6) were recorded on Varian Unity Invoa 400 MHz. The ^{1}H NMR data are reported as peak multiplicities: s for singlet, d for doublet, dd for doublet of doublets, t for triplet, q for quartet, br s for broad singlet, and m for multiplet. Coupling constants are reported in hertz. ^{13}C NMR ($CDCl_3$, CD_3OD, or DMSO-d_6) spectra were recorded on Varian Unity Inova 100 MHz. ^{19}F NMR ($CDCl_3$, CD_3OD) were recorded on Varian Unity Inova 376 MHz. The chemical shifts were reported as parts per million (δ) relative to the solvent peak. Optical rotations were determined on Jasco III in the appropriate solvent. UV spectra were recorded on U-3000 made by Hitachi in methanol or water. Infrared spectra were recorded on FT-IR (FTS-135) made by Bio-Rad. Melting points were measured on B-540 made by Buchi. Elemental analyses (C, H, and N) were used to determine the purity of all synthesized compounds, and the results were within $\pm$0.4% of the calculated values, confirming $\geq$95% purity. Reactions were checked with TLC (Merck precoated 60F_{254} plates). Spots were detected by viewing under a UV light, colorizing with charring after dipping in anisaldehyde solution with acetic acid, sulfuric acid, and methanol. Column chromatography was performed on silica gel 60 (230−400 mesh, Merck). Reagents were purchased from Aldrich Chemical Co. Solvents were obtained from local suppliers. All the anhydrous solvents were distilled over CaH_2, P_2O_5, or sodium/benzophenone prior to the reaction.

Synthesis. See the Supporting Information for full experimental procedure.

5-(6-Aminopurin-9-yl)-4-fluoro-3-hydroxymethylcyclopent-3-ene-1,2-diol (4b, X = CH_2OH, Y = F):[5] yield = 77%; MS (FAB) m/z 282 (M + H$^+$); mp 181−184 °C; $[\alpha]_D^{25}$ −181.1° (c 0.62, MeOH); UV (H_2O) λ_{max} 260.0 nm; ^{1}H NMR (CD_3OD) δ 8.17 (s, 1 H), 8.15 (s, 1 H), 5.56 (br s, 1 H), 4.79 (pseudo t, J = 5.2, 6.0 Hz, 1 H), 4.56 (t, J = 5.6 Hz, 1 H), 4.41 (d, J = 13.2 Hz, 1 H), 4.16 (td, J = 2.4, 13.2 Hz, 1 H); ^{13}C NMR (CD_3OD) δ 157.7, 154.7 (d, J = 285.3 Hz), 154.2, 151.2, 142.1, 122.8 (d, J = 2.3 Hz), 120.8, 75.7 (d, J = 4.6 Hz), 71.2 (d, J = 8.5 Hz), 63.6 (d, J = 18.4 Hz), 54.7; ^{19}F NMR (CD_3OD) δ −133.1. Anal. Calcd for $C_{11}H_{12}FN_5O_3$: C, 46.98; H, 4.30; N, 24.90. Found: C, 46.99; H, 4.28; N, 25.20.

5-(6-Aminopurin-9-yl)-4-chloro-3-hydroxymethylcyclopent-3-ene-1,2-diol (4c, X = CH_2OH, Y = Cl): yield = 64%; MS (FAB) m/z 299 (M + H$^+$); mp 250.7−251.0 °C; $[\alpha]_D^{25}$ −20.0° (c 1.14, DMSO); UV (MeOH) λ_{max} 265.0 nm; MS (FAB) m/z 299 (M + H$^+$); ^{1}H NMR (DMSO-d_6) δ 8.18 (s, 1 H), 8.12 (s, 1 H), 7.25 (s, 1 H), 5.42 (d, J = 5.6 Hz, 1 H), 5.40 (d, J = 6.4 Hz, 1 H), 5.21 (d, J = 5.6 Hz, 1 H), 5.05 (t, J = 5.6 Hz, 1 H), 4.63−4.60 (m, 2 H), 4.21 (d, J = 13.2 Hz, 1 H), 4.06 (d, J = 13.2 Hz, 1 H); ^{13}C NMR (DMSO-d_6) δ 156.6, 153.2, 150.5, 143.0, 141.1, 127.9, 119.7, 74.4, 70.9, 67.0, 55.7. Anal. Calcd for $C_{11}H_{12}ClN_5O_3$: C, 44.38; H, 4.06; N, 23.53. Found: C, 44.40; H, 4.08; N, 23.40.

5-(6-Aminopurin-9-yl)-4-bromo-3-hydroxymethyl-cyclopent-3-ene-1,2-diol (4d, X = CH_2OH, Y = Br): yield = 87%; MS (FAB) m/z 343 (M + H$^+$); mp 240.1−241.8 °C; $[\alpha]_D^{25}$ −14.2° (c 1.26, MeOH); UV (MeOH) λ_{max} 260.5 nm; MS (FAB) m/z 343 (M + H$^+$); ^{1}H NMR (CD_3 OD) δ 8.18 (s, 1 H), 8.15 (s, 1 H), 5.55 (dt, J = 1.4, 6.0 Hz, 1 H), 4.83 (s, 1 H), 4.70 (t, J = 6.0 Hz, 1 H), 4.40 (d, J = 13.2 Hz, 1 H), 4.26 (dd, J = 2.8, 13.2 Hz, 1 H); ^{13}C NMR (DMSO-d_6) δ 156.0, 152.5, 149.8, 145.8, 140.4, 119.3, 119.1, 74.1, 70.9, 67.5, 57.0. Anal. Calcd for $C_{11}H_{12}BrN_5O_3$: C, 38.61; H, 3.54; N, 20.47. Found: C, 38.66; H, 3.58; N, 20.54.

5-(6-Aminopurin-9-yl)-4-iodo-3-hydroxymethylcyclopent-3-ene-1,2-diol (4e, X = CH_2OH, Y = I):[17] yield = 62%; MS (FAB) m/z 390 (M + H$^+$); mp 168.2−172.5 °C; $[\alpha]_D^{25}$ −100.6° (c 0.83, MeOH); UV (MeOH) λ_{max} 260.0 nm; ^{1}H NMR (CD_3OD) δ 8.42 (s, 1 H), 8.41 (s, 1 H), 5.67 (d, J = 5.0 Hz, 1 H), 4.85 (d, J = 6.0 Hz, 1 H), 4.69 (t, J = 6.0 Hz, 1 H), 4.34 (brd, J = 13.0 Hz, 1 H), 4.29 (d, J = 13.0 Hz, 1 H); ^{13}C NMR (CD_3OD) δ 154.5, 151.9, 150.8, 145.4, 145.1, 120.5, 98.2, 77.1, 73.6, 73.2, 62.3. Anal. Calcd for $C_{11}H_{12}IN_5O_3$: C, 33.95; H, 3.11; N, 18.00. Found: C, 33.83; H, 3.18; N, 17.87.

5-(6-Aminopurin-9-yl)-4-fluorocyclopent-3-ene-1,2-diol (5b, X = H, Y = F):[9] yield = 92%; MS (FAB) m/z 252 (M + H$^+$); $[\alpha]_D^{25}$ −172.4° (c 0.77, MeOH); UV (MeOH) λ_{max} 259.0 nm; ^{1}H NMR (CD_3OD) δ 8.19 (s, 1 H), 8.18 (s, 1 H), 5.63 (m, 1 H), 5.60 (m, 1 H), 4.75 (m, 1 H), 4.68 (td, J = 1.2, 6.0 Hz, 1 H); ^{13}C NMR (CD_3OD) δ 162.1, 159.3, 157.4, 153.8, 151.2, 142.1, 120.7, 110.1 (d, J = 4.9 Hz), 76.6 (d, J = 4.2 Hz), 70.7 (d, J = 10.4 Hz), 62.9 (d, J = 18.2 Hz); ^{19}F NMR (CD_3OD) δ −121.6. Anal. Calcd for $C_{10}H_{10}FN_5O_2$: C, 47.81; H, 4.01; N, 27.88. Found: C, 47.96; H, 4.08; N, 28.04.

5-(6-Aminopurin-9-yl)-4-chlorocyclopent-3-ene-1,2-diol (5c, X = H, Y = Cl): yield = 83%; MS (FAB) m/z 269 (M + H$^+$); UV (MeOH) λ_{max} 260.0 nm; MS (FAB) m/z 268 (M + H$^+$); ^{1}H NMR (DMSO-d_6) δ 8.22 (s, 1 H), 8.11 (s, 1 H), 7.29 (br s, 2 H), 6.28 (t, J = 2.4 Hz, 1 H), 5.44 (m, 2 H), 5.26 (d, J = 6.0 Hz, 1 H), 4.67 (dd, J = 5.6, 6.0 Hz, 1 H), 4.57 (m, 1 H); ^{13}C NMR (DMSO-d_6) δ 156.7, 156.6, 153.2, 150.4, 141.3, 134.7, 132.6, 75.2, 71.3, 66.7. Anal. Calcd for $C_{10}H_{10}ClN_5O_2$: C, 44.87; H, 3.77; N, 26.16. Found: C, 44.71; H, 3.95; N, 26.03.

5-(6-Aminopurin-9-yl)-4-bromocyclopent-3-ene-1,2-diol (5d, X = H, Y = Br): yield = 99%; MS (FAB) m/z 313 (M + H$^+$); mp 115.1−120.4 °C; $[\alpha]_D^{25}$ −118.7° (c 1.20, MeOH); UV (MeOH) λ_{max} 260.0 nm; ^{1}H NMR (CD_3OD) δ 8.18 (s, 1 H), 8.16 (s, 1 H), 6.47 (dd, J = 2.0, 2.8 Hz, 1 H), 5.55 (ddd, J = 1.6, 2.0, 6.0 Hz, 1 H), 4.76 (t, J = 6.0 Hz, 1 H), 4.70 (ddd, J = 1.6, 2.8, 6.0 Hz, 1 H); ^{13}C NMR (CD_3OD) δ 157.4, 153.8, 151.1, 142.2, 137.7, 126.6, 120.6, 76.7, 73.7, 69.82. Anal. Calcd for $C_{10}H_{10}BrN_5O_2$: C, 38.48; H, 3.23; N, 22.44. Found: C, 38.61; H, 3.34; N, 22.46.

5-(6-Aminopurin-9-yl)-4-iodocyclopent-3-ene-1,2-diol (5e, X = H, Y = I): yield = 96%; MS (FAB) m/z 360 (M + H$^+$); mp 119.4−124.8 °C; $[\alpha]_D^{25}$ −55.6° (c 1.30, MeOH); UV (MeOH) λ_{max} 260.5 nm; ^{1}H NMR (CD_3OD) δ 8.18 (s, 1 H), 8.15 (s, 1 H), 6.72 (dd, J = 2.0, 2.8 Hz, 1 H), 5.52 (ddd, J = 12, 2.0, 6.0 Hz, 1 H), 4.75 (t, J = 6.0 Hz, 1 H), 4.65 (ddd, J = 1.2, 2,8, 6.0 Hz, 1 H); ^{13}C NMR (CD_3OD) δ 157.3, 153.5, 151.0, 146.0, 142.3, 120.6, 101.9, 76.2, 75.1, 72.4. Anal. Calcd for $C_{10}H_{10}IN_5O_2$: C, 33.44; H, 2.81; N, 19.50. Found: C, 33.56; H, 2.99; N, 19.42.

Enzyme Assay. Materials. *S*-Adenosyl-L-homocysteine (AdoHcy) and homocysteine thiolactone were purchased from Sigma. Co. Adenosine was obtained from BDH Chemical Co. Dr. Michael S. Hershfield (Duke Univ.) kindly provided the plasmic pPROKcd20 containing cloned gene of human placental AdoHcy hydrolase. *E. coli* JM109 was obtained from KTCC (Korea Type Culture Collection).

Purification of AdoHcy Hydrolase. The cloned human placental AdoHcy hydrolase was purified from the cell-free extracts of *E. coli* JM109 containing the plasmid pPROKcd20 grown in 2xYT medium with IPTG induction.[18] The cell-free extracts were obtained by sonication of a cell suspension of *E. coli* JM109 containing pPROKcd20 in 50 mM Tris-HCl (pH 7.5) containing 2 mM EDTA.

The purification was carried out through DEAE-cellulose column (2.8 cm × 6 cm), ammonium sulfate fractionation

(35−60%), Sephacryl S-300HR (1.0 cm × 105 cm), and DEAE-cellulose (2.8 cm × 24 cm). The protein homogeneity was confirmed by 10% SDS−PAGE. The protein concentration was determined by using Bradford method.[19] Bovine serum albumin was a standard material for protein assay.

Assay of AdoHcy Hydrolase for Synthetic Direction. The enzyme was incubated with 0.2 mM Ado and 5 mM Hcy in 500 μL of 50 mM potassium phosphate buffer (pH 7.2) containing 1 mM EDTA (buffer A) at 37 °C for 5 min. The reaction was terminated by the addition of 25 μL of 5 N $HClO_4$. The terminated reaction mixture was kept in ice for 5 min and microcenrifuged. The supernatant was analyzed for AdoHcy by HPLC equipped C-18 reversed-phase column (Econosphere C18, 5 μm, 250 mm × 4.6 mm, Alltech, Deerfield, IL). The elution was carried out at a flow rate of 1 mL/min in two sequential linear gradients: 6−15% A over 15 min, 15−50% A over the next 5 min, where mobile phase A was acetonitrile and B was 50 mM sodium phosphate buffer (NaH_2PO_4/H_3PO_4), pH 3.2 (HPLC buffer B). The peak of AdoHcy was monitored at 258 nm. The concentration was determined by the peak area of AdoHcy.

Concentration-Dependent Inactivation of AdoHcy Hydrolase (Figure S1). Various concentrations of each inhibitor were incubated with AdoHcy hydrolase (400 nM) in buffer A at 37 °C for 5 min, and the remaining activity was determined in the synthetic direction as described above.

Time- and Concentration-Dependent Inactivations of AdoHcy Hydrolase (Figure S2). Various concentrations of active compounds (**4b**−**d** and **5b**) were incubated with AdoHcy hydrolase (184 nM) in buffer A at 37 °C for different amounts of time (5, 8, or 10 min), and the remaining activity was determined in the synthetic direction as described above.

Determination of Irreversibility of AdoHcy Hydrolase Activity (Figure S3). The enzyme (400 nM) was preincubated with active compounds (**4b**−**d** and **5b**) at 37 °C for 5 min. It was dialyzed through Centricon 30 up to 90 fold. During dialysis, AdoHcy hydrolase activity was determined in the synthetic direction as described above.

Crystallization, X-ray Data Collection, and Structure Determination. For crystallization, we added fluoroneplanocin A and NAD^+ to the concentrated protein solution to give a fluoroneplanocin A/NAD^+/protein molar ratio of 10:5:1 and incubated the mixture for 1 h at 277 K. The incubated protein was crystallized at 20 °C by vapor diffusion using the hanging-drop method and a protein to reservoir solution ratio of 1:1, with the reservoir solution containing 0.1 M lithium sulfate, 0.1 M HEPES (pH 8.0), and 20% PEG400. Prior to X-ray data collection, crystals were transferred to the cryoprotectant solution containing the reservoir solution plus 20% (v/v) glycerol for a few seconds, then looped from the drop and flash-frozen in liquid nitrogen. The X-ray diffraction data for the crystal were collected at the 6B beamline of Pohang Light Source (PLS) and processed using HKL2000.[20] The crystal belongs to the space group $P2_1$, and the unit cell parameters are a = 91.201 Å, b = 75.80 Å, c = 189.01 Å, and β = 107.01°.

The structure was solved by molecular replacement (MR) using the program CNS[21] with the previously reported structure (PDB code 1A7A)[11] as a search model. Using the data with a resolution range of 50.0−2.5 Å, the MR solution structure was refined with the CNS package and manual model building was performed using the program Coot.[22] During refinement, 5% of reflection data chosen randomly from the observed data were used for cross-validation with the R_{free} value. The coordinates and structure factors have been deposited in PDB (http://www.rcsb.org/pdb) under the accession code of 3NJ4. The statistics for data collection and structure refinement are given in Table S2 in the Supporting Information.

Molecular Modeling. X-ray Crystal Structure Preparation and Flexible Docking. X-ray crystal structure was prepared with clean module in Discovery Studio, version 2.5 package (Accelrys, San Diego, CA, U.S.) including the addition of hydrogen atoms and charges appropriate to pH 7.0, and His55 residue was set to be protonated in its N_{E2} position. Then the flexible docking study was performed using GOLD, version 4.1 (Cambridge Crystallographic Data Centre, U.K.), in the defined binding site at 10 Å from the crystal ligand. Ten residues in the binding site were selected and set to be flexible with "crystal mode", defining a rotamer in which all rotatable torsions in the side chain are allowed to vary over the range ($\delta - \chi$) to ($\delta + \chi$), where χ values are taken from the protein input file. The selected 10 residues were His55, Glu156, His301, Leu344, Asn346, and Leu347 with δ of 20 and Asp131, Thr157, Lys186, and Asp190 with δ of 10. Other options were set to default except GA (genetic algorithm) runs of 30. Among the resulting docked conformations, reasonable complexes with high GOLD fitness scores were selected and energy minimized using CHARMm program, implemented in Discovery Studio, version 2.5. By application of harmonic restraints with a force constant of 10 to backbone atoms of the residues beyond 5 Å from the ligand and heavy atoms of the cofactor, the system was minimized with the conjugate gradient algorithm until the rms gradient tolerance reached 0.01 kcal/(mol·Å) (max steps of 10 000).

Homology Modeling. Homology model of the open form human AdoHcy hydrolase was built by MODELER implemented in Discovery Studio, version 2.5, using the open form structure of rat AdoHcy hydrolase (PDB code 1B3R)[12] as a template. Among the 30 models generated with the high optimization level, the initial model was selected by the lowest probability density function (PDF) total energy and refined using molecular dynamics (MD) simulation and energy minimization. MD simulation was conducted via standard dynamics cascade protocol in Discovery Studio, version 2.5, followed by 500 steps of minimization with steepest descent (rms gradient of 0.1 kcal/(mol·Å)), 500 steps of minimization with conjugate gradient (rms gradient of 0.0001 kcal/(mol·Å)), 2000 steps of heating, 4000 steps of equilibration, and finally 10 000 steps of production phase with an NVE ensemble at 300 K. During the simulation, an integration time step of 0.001 ps (1 fs) was used, and harmonic restraints with force constant of 10 were applied to the backbone of the identical residues and heavy atoms of the cofactor. In addition, harmonic restraints with a force constant of 5 were also applied to side chain heavy atoms of the identical residues located in the interface during heating, equilibration, and production phase. The resulting conformation in final trajectory was further energy minimized with the conjugate gradient algorithm (max steps of 10 000; rms gradient of 0.01 kcal/(mol·Å)), and the final refined model was validated by the Verify Protein (Profiles-3D) module in Discovery Studio, version 2.5.

Binding Energy Calculation. The potential energies of each complex and the refined homology model were calculated, and the relative binding energy was estimated by eq 1. Energy values of the complexes and the holoenzyme were obtained from the docked and minimized systems and the refined homology model, respectively. For free ligands that are not bound in the enzyme, their potential energies were calculated using conjugate gradient with max steps of 1 000 000 and rms gradient of 0.01 kcal/(mol·Å).

All the computational studies were performed on a Linux (Cent OS, release 4.6) workstation. During the minimization and MD simulations, the CHARMm force field and implicit solvent model, generalized Born with molecular volume (GBMV), were used and the bond lengths involving bonds to hydrogen atoms were constrained by the SHAKE algorithm. The resulting figures were generated in the SYBYL molecular modeling program, version 8.1.1 (Tripos International, St. Louis, MO, U.S.).

Acknowledgment. This work was supported by grants from the WCU program (Grant R31-2008-000-10010-0) and

the National Core Research Center (NCRC) program (Grant R15-2006-020) of the National Research Foundation (NRF) of Korea. H.W.L. acknowledges a Research Professor Fellowship from Ewha Womans University (2009).

Supporting Information Available: Additional experimental procedures and characterization data for all unknown compounds; X-ray crystallographic results; enzyme assay results. This material is available free of charge via the Internet at http://pubs.acs.org.

References

(1) (a) Turner, M. A.; Yang, X.; Yin, D.; Kuczera, K.; Borchardt, R. T.; Howell, P. L. Structure and function of *S*-adenosylhomocysteine hydrolase. *Cell Biochem. Biophys.* **2000**, *33*, 101–125. (b) Cantoni, G. L. The Centrality of S-Adenosylhomocysteinase in the Regulation of the Biological Utilization of S-Adenosylmethionine. In *Biological Methylation and Drug Design*; Borchardt, R. T., Creveling, C. R., Ueland, P. M., Eds.; Humana Press: Clifton, NJ, 1986; pp 227−238.

(2) (a) Snoeck, R.; Andrei, G.; Neyts, J.; Schols, D.; Cools, M.; Balzarini, J.; De Clercq, E. Inhibitory activity of *S*-adenosylhomocysteine hydrolase inhibitors against human cytomegalovirus replication. *Antiviral Res.* **1993**, *21*, 197–216. (b) Liu, S.; Wolfe, M. S.; Borchardt, R. T. Rational approaches to the design of antiviral agents based on S-adenosyl-L-homocysteine hydrolase as a molecular target. *Antiviral Res.* **1992**, *19*, 247–265.

(3) Wolfe, M. S.; Borchardt, R. T. *S*-Adenosyl-L-homocysteine hydrolase as a target for antiviral chemotherapy. *J. Med. Chem.* **1991**, *34*, 1521–1530.

(4) Keller, B. T.; Borchardt, R. T. Metabolism and Mechanism of Action of Neplanocin A: A Potent Inhibitor of *S*-Adenosylhomocysteine Hydrolase. In *Biological Methylation and Drug Design*; Borchardt, R. T., Creveling, C. R., Ueland, P. M., Eds.; Humana Press: Clifton, NJ, 1986; pp 385−396.

(5) Jeong, L. S.; Yoo, S. J.; Lee, K. M.; Koo, M. J.; Choi, W. J.; Kim, H. O.; Moon, H. R.; Lee, M. Y.; Park, J. G.; Lee, S. K.; Chun, M. W. Design, synthesis, and biological evaluation of fluoroneplanocin A as the novel mechanism-based inhibitor of *S*-adenosylhomocysteine hydrolase. *J. Med. Chem.* **2003**, *46*, 201–203.

(6) The preliminary accounts were published in the Proceedings of XV International Roundtable, Leuven, Belgium, September 10−14, 2002. (a) Jeong, L. S.; Moon, H. R.; Park, J. G.; Shin, D. H.; Choi, W. J.; Lee, K. M.; Kim, H. O.; Chun, M. W.; Kim, H. D.; Kim, J. H. Synthesis and biological evaluation of halo-neplanocin A as novel mechanism-based inhibitors of *S*-adenosylhomocysteine hydrolase. *Nucleosides, Nucleotides Nucleic Acids* **2003**, *22*, 589–592. (b) Jeong, L. S.; Park, J. G.; Choi, W. J.; Moon, H. R.; Lee, K. M.; Kim, H. O.; Kim, H. D.; Chun, M. W.; Park, H. Y.; Kim, K.; Sheen, Y. Y. Synthesis of halogenated 9-(dihydroxycyclopent-4′-enyl) adenines and their inhibitory activities against S-adenosylhomocysteine hydrolase. *Nucleosides, Nucleotides Nucleic Acids* **2003**, *22*, 919–921.

(7) Moon, H. R.; Choi, W. J.; Kim, H. O.; Jeong, L. S. Preparative synthesis of the key intermediate, (4*R*,5*R*)-3-benzyloxymethyl-4,5-isopropylidenedioxycyclopent-2-enone for carbocyclic nucleosides. *Chem. Lett.* **2004**, *33*, 506–507.

(8) Moon, H. R.; Choi, W. J.; Kim, H. O.; Jeong, L. S. Improved and alternative synthesis of D- and L-cyclopentenone derivatives, the versatile intermediates for the synthesis of carbocyclic nucleosides. *Tetrahedron: Asymmetry* **2002**, *13*, 1189–1193.

(9) Kim, H. O.; Yoo, S. J.; Ahn, H. S.; Choi, W. J.; Moon, H. R.; Lee, K. M.; Chun, M. W.; Jeong, L. S. Synthesis of fluorinated cyclopentenyladenine as potent inhibitor of *S*-adenosylhomocysteine hydrolase. *Bioorg. Med. Chem. Lett.* **2004**, *14*, 2091–2093.

(10) Yang, X. D.; Hu, Y. B.; Yin, D. H.; Turner, M. A.; Wang, M.; Borchardt, R. T.; Howell, P. L.; Kuczera, K.; Schowen, R. L. Catalytic strategy of *S*-adenosyl-L-homocysteine hydrolase: transition-state stabilization and the avoidance of abortive reactions. *Biochemistry* **2003**, *42*, 1900–1909.

(11) Turner, M. A.; Yuan, C. S.; Borchardt, R. T.; Hershfield, M. S.; Smith, G. D.; Howell, P. L. Structure determination of selenomethionyl *S*-adenosylhomocysteine hydrolase using data at a single wavelength. *Nat. Struct. Biol.* **1998**, *5*, 369–376.

(12) Hu, Y. B.; Komoto, J.; Huang, Y.; Gomi, T.; Ogawa, H.; Takata, Y.; Fujioka, M.; Takusagawa, F. Crystal structure of *S*-adenosylhomocysteine hydrolase from rat liver. *Biochemistry* **1999**, *38*, 8323–8333.

(13) (a) Stepkowski, T.; Brzezinski, K.; Legocki, A. B.; Jaskolski, M.; Bena, G. Bayesian phylogenetic analysis reveals two-domain topology of *S*-adenosylhomocysteine hydrolase protein sequences. *Mol. Phylogenet. Evol.* **2005**, *34*, 15–28. (b) Reddy, M. C. M.; Kuppan, G.; Shetty, N. D.; Owen, J. L.; Ioerger, T. R.; Sacchettini, J. C. Crystal structures of Mycobacterium tuberculosis S-adenosyl-L-homocysteine hydrolase in ternary complex with substrate and inhibitors. *Protein Sci.* **2008**, *17*, 2134–2144.

(14) Tanaka, N.; Nakanishi, M.; Kusakabe, Y.; Shiraiwa, K.; Yabe, S.; Ito, Y.; Kitade, Y.; Nakamura, K. T. Crystal structure of *S*-adenosyl-L-homocysteine hydrolase from the human malaria parasite *Plasmodium falciparum*. *J. Mol. Biol.* **2004**, *343*, 1007–1017.

(15) Yamada, T.; Takata, Y.; Komoto, J.; Gomi, T.; Ogawa, H.; Fujioka, M.; Takusagawa, F. Catalytic mechanism of *S*-adenosylhomocysteine hydrolase: roles of His 54, Asp130, Glu155, Lys185, and Asp189. *Int. J. Biochem. Cell Biol.* **2005**, *37*, 2417–2435.

(16) Rowland, R. S.; Taylor, R. Intermolecular nonbonded contact distances in organic crystal structures: comparison with distances expected from van der Waals radii. *J. Phys. Chem.* **1996**, *100*, 7384–7391.

(17) Park, A.-Y.; Kim, K. R.; Lee, H.-R.; Kang, J.-A.; Kim, W. H.; Chun, P.; Ahmad, P.; Jeong, L. S.; Moon, H. R. Design and synthesis of 5″-iodoneplanocin A and its analogues as potential *S*-adenosylhomocysteine hydrolase inhibitor. *Bull. Korean Chem. Soc.* **2008**, *29*, 2487–2490.

(18) Yuan, C. S.; Yeh, J.; Liu, S.; Borchardt, R. T. Mechanism of inactivation of *S*-adenosylhomocysteine hydrolase by (*Z*)-4′,5′-didehydro-5′-deoxy-5′-fluoroadenosine. *J. Biol. Chem.* **1993**, *268*, 17030–17037.

(19) Bradford, M. M. A rapid and sensitive method for the quantitation of microgram quantities of protein utilizing the principle of protein−dye binding. *Anal. Biochem.* **1976**, *72*, 248–254.

(20) Otwinowski, Z.; Minor, W. Processing of X-ray Diffraction Data Collected in Oscillation Mode. In *Macromolecular Crystallography. Part A*; Carter, C. W., Sweet, R. M., Eds.; Methods in Enzymology, Vol. 276; Academic Press: San Diego, CA, 1997; pp 307−326.

(21) Brunger, A. T.; Adams, P. D.; Clore, G. M.; DeLano, W. L.; Gros, P.; Grosse-Kunstleve, R. W.; Jiang, J. S.; Kuszewski, J.; Nilges, M.; Pannu, N. S.; Read, R. J.; Rice, L. M.; Simonson, T.; Warren, G. L. Crystallography & NMR system: a new software suite for macromolecular structure determination. *Acta Crystallogr., Sect. D: Biol. Crystallogr.* **1998**, *54*, 905–921.

(22) Emsley, P.; Cowtan, K. Coot: model-building tools for molecular graphics. *Acta Crystallogr., Sect. D: Biol. Crystallogr.* **2004**, *60*, 2126–2132.